iScience

CellPress
OPEN ACCESS

Article

Cost-effective high-speed, three-dimensional live-cell imaging of HIV-1 transfer at the T cell virological synapse

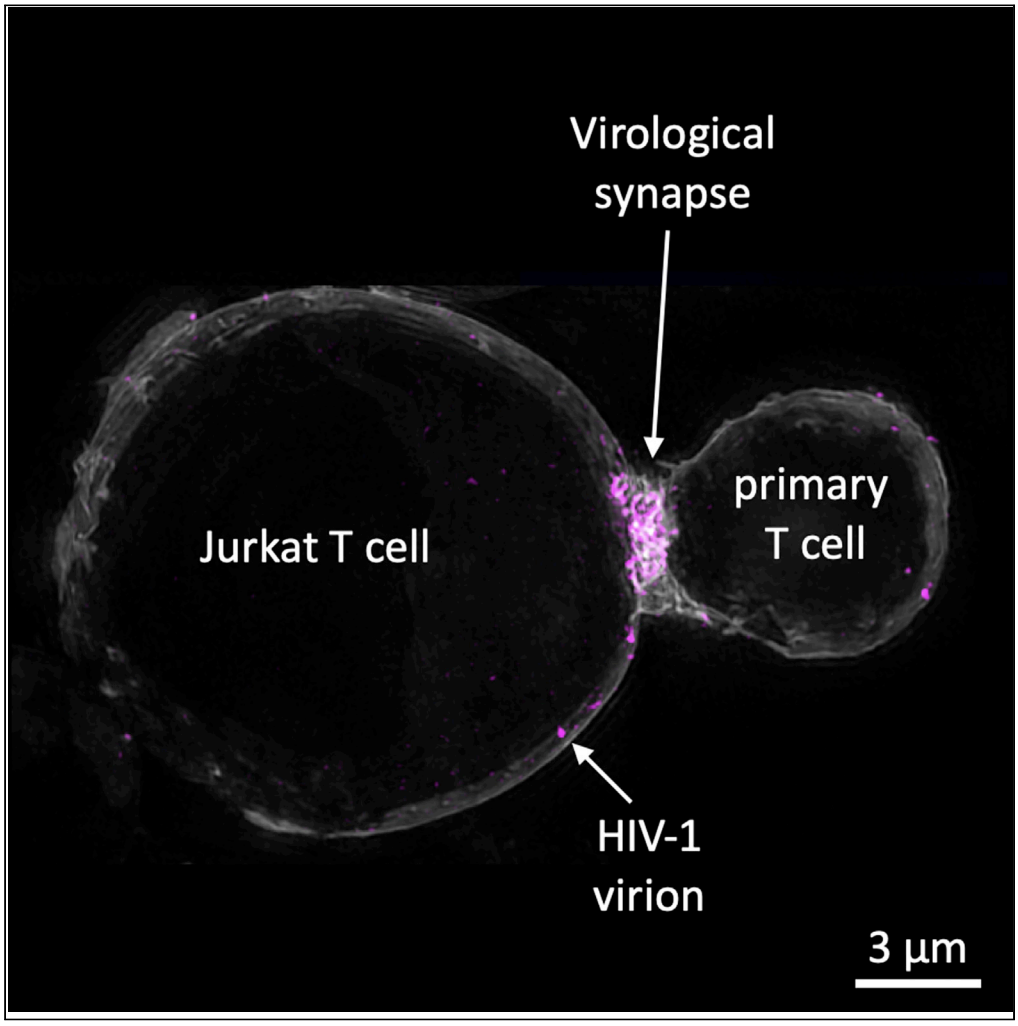

Alice Sandmeyer, Lili Wang, Wolfgang Hübner, Marcel Müller, Benjamin K. Chen, Thomas Huser

benjamin.chen@mssm.edu (B.K.C.)
thomas.huser@physik.uni-bielefeld.de (T.H.)

Highlights

A cost-effective, high-speed 3D fluorescence microscope was developed

Three-dimensional fluorescence micrographs of immune cells were collected

Transfer of HIV-1 between infected and uninfected T cells was observed

Super-resolution SIM imaging revealed HIV-1 particles in immunological synapses

Sandmeyer et al., iScience 25, 105468
November 18, 2022
https://doi.org/10.1016/j.isci.2022.105468

iScience

CellPress
OPEN ACCESS

Article

Cost-effective high-speed, three-dimensional live-cell imaging of HIV-1 transfer at the T cell virological synapse

Alice Sandmeyer,[1] Lili Wang,[2] Wolfgang Hübner,[1] Marcel Müller,[1] Benjamin K. Chen,[2,*] and Thomas Huser[1,3,*]

SUMMARY

The availability of cost-effective, highly portable, and easy to use high-resolution live-cell imaging systems could present a significant technological break-through in challenging environments, such as high-level biosafety laboratories or sites where new viral outbreaks are suspected. We describe and demonstrate a cost-effective high-speed fluorescence microscope enabling the live tracking of virus particles across virological synapses that form between infected and uninfected T cells. The dynamics of HIV-1 proteins studied at the cellular level and the formation of virological synapses in living T cells reveals mechanisms by which cell-cell interactions facilitate infection between immune cells. Dual-color 3D fluorescence deconvolution microscopy of HIV-1 particles at frames rates of 100 frames per second allows us to follow the transfer of HIV-1 particles across the T cell virological synapse between living T cells. We also confirm the successful transfer of virus by imaging T cell samples fixed at specific time points during cell-cell virus transfer by super-resolution structured illumination microscopy.

INTRODUCTION

High-speed and high-resolution optical fluorescence microscopy of living, virus-infected cells is still a challenge for most infectious disease research laboratories, as this typically requires the installation of expensive, bulky, and maintenance-intensive equipment (e.g. laser-scanning microscopes) in high-level biosafety laboratories. Imaging individual cells with high speed and high spatial (albeit diffraction-limited) resolution currently requires the use of microscope objective lenses with high numerical aperture (NA). Yet, only highly sensitive fluorescence microscopes are able to track single fluorescent viruses with a size of 120 nm or less, and only super-resolution optical microscopes can resolve such viruses in living cells.[1] The tracking of virus movement within an infected cell and its transmission from infected to uninfected cells complicates this even more, because in this case these highly active and nonadherent cells have to be imaged with high sensitivity and at high speed in 3D. Up to date, spinning-disk confocal microscopes are among the most prominent choice for rapidly imaging the full cell volume, but these microscopes are rather specialized systems; newer generations are hermetically sealed, preventing servicing or adaptations by the user or their transfer in and out of high-level biosafety laboratories, which requires decontamination, and their operation requires additional state-of-the art equipment, e.g. high-end PC workstations for data processing and analysis.[2,3]

Imaging the transfer of individual particles of the HIV at direct cell-to-cell contacts between T cells via fluorescence microscopy is particularly challenging, because the virus affects and spreads between immune cells, which are typically nonadherent and circulate in the blood at high velocity. Even when isolated from the blood, these cells remain highly motile and can translate, roll, or rotate on the millisecond to second timescale.[4] HIV causes the acquired immune deficiency Syndrome (AIDS) and currently approximately 38 million people worldwide are infected with this deadly virus.[5] The dissemination pathway of HIV through virological synapses (VS) is still under investigation, and it remains elusive how cell-cell interactions contribute to the infectious process.[6] A key aspect is the formation of the VS, which is an adhesive structure between an HIV-infected cell and a target cell and through which the virus transfers directly into the target cell.[7,8] In the case of T cell-to-T cell transfer, the VS is initiated through the interaction of the viral envelope glycoprotein (Env) at the surface of the infected cell and the CD4 receptor expressed by the target cell. The virus then assembles specifically at the VS, buds, and is endocytosed by the previously uninfected cell.[2,8]

[1]Biomolecular Photonics, Faculty of Physics, Bielefeld University, 33615 Bielefeld, Germany

[2]Division of Infectious Diseases, Department of Medicine, Icahn School of Medicine at Mount Sinai, New York City, NY 10029, USA

[3]Lead contact

*Correspondence: benjamin.chen@mssm.edu (B.K.C.), thomas.huser@physik.uni-bielefeld.de (T.H.)

https://doi.org/10.1016/j.isci.2022.105468

The infection, though, occurs only after maturation of the virus particles within the endocytic compartments.[9,10] The direct transfer by cell-to-cell contact allows for multiple infection events of a single host cell and is therefore much more efficient at transferring viral antigen to target cells than the free particle plasma membrane fusion mechanism.[2,11]

A number of commercial systems for advanced fluorescence microscopy that also incorporate sophisticated contrast generating techniques, such as optical super-resolution imaging, exist. However, for a single research group or small facilities, the cost of installing and operating just one such advanced imaging system is often too high, not to mention the cost of several systems. Thus, various concepts were developed to democratize fluorescence microscopy and enable their installation and operation in challenging environments. For this purpose, cost-efficiency and easy to replicate solutions[12] are key to guaranteeing that a wide range of scientists can have access to techniques such as optical super-resolution microscopy[13–15] or advanced wide-field microscopy[16,17] in order to perform their experiments. For the last several years, compact and inexpensive fluorescence microscopes have been reported and have also become available from commercial sources, and they are great accessories for typical cell biology laboratories.[18–22] These microscopes provide wide-field imaging capability with limited sensitivity and imaging speed (typically 10 frames per second [fps] up to 24 fps) and some even permit 3D imaging. Commercial fluorescence microscopes are, however, typically tightly integrated systems, which are difficult to take apart and decontaminate if they are in need of repair or have to be removed from biosafety laboratories.

Here, we report on the development and the application of a cost-effective wide-field fluorescence microscope specifically developed for high-speed 3D imaging of living, HIV-1-infected T cells. We previously demonstrated that HIV-1 puncta in the host cell move at speeds of up to 0.8 μm/s to the VS and that the compartments receiving virus particles in the target cell are 1–2 μm in diameter. The 3D imaging process for an entire virus-expressing cell takes on the order of 1–1.5 s. This explains the need for high-spatial resolution (<0.5 μm), high-sensitivity (a single fluorescent molecule can be imaged within 10 ms acquisition time with the camera used in the system), and high-speed (100 fps) microscope system imaging the transfer of HIV-1 particles.[15,23] Furthermore, the system is compact, versatile, and easy to assemble, disassemble, and service, and its components can be disinfected in an autoclaved if needed. This system was developed as part of a cross-continental collaboration with the imaging group residing in Germany and the infectious disease research group residing in the United States. We demonstrate that this compact and cost-effective system is able to successfully image HIV-1 transfer across VS from living infected T cells to previously uninfected primary T cells in 3D and for extended periods of time. Our findings are further verified by imaging this process at various time points by super-resolution structured illumination microscopy of fixed T cells. This work is an essential contribution toward global efforts of placing advanced optical microscopes in the hands of biologists, in particular infectious disease researchers.

RESULTS

Development of a cost-effective, compact, high-speed and high-resolution fluorescence microscope for 4D imaging of living T cells

We developed a compact fluorescence microscope, which was specifically designed to provide diffraction-limited optical resolution, high sensitivity, and high-speed imaging while still utilizing cost-efficient components. The system resembles an open-frame wide-field fluorescence microscopy setup that is specifically optimized to permit fast 3D image acquisition. Such compact microscope systems can now be realized by utilizing uncooled industry-grade cameras (IDS μEye UI-3060CP-M, IDS, Germany), which have been demonstrated to achieve single molecule fluorescence detection sensitivity,[14,15,24,25] while substantially reducing the overall cost of the system. The microscope itself consists of two stacked aluminum optics breadboards, which further decreases the overall footprint of the system so that it can be easily shipped (see Figure 1A). Fast z-scanning through the sample is achieved by moving the objective lens along the optical axis via a piezo-electric translation stage (PiFoc P-721, Physik Instrumente, Germany; Figures 1A–1C). The lower optics board (Figures 1D and 1E) can be defined as a laser combiner, where an acousto-optic tunable filter (AOTF, AA Optoelectronics, France) allows for fast switching and power control of two solid-state lasers (Figures 1D and 1E). The wavelengths of the lasers (473 and 561 nm) were chosen such that the fluorescent proteins green fluorescent protein (GFP) and mCherry can be selectively excited. In order to allow for prolonged live-cell imaging, a sample heating chamber was also designed and integrated into the microscope. To demonstrate the sensitivity and spatial resolution, the image of a 100 nm fluorescent bead was acquired and is shown as an insert in

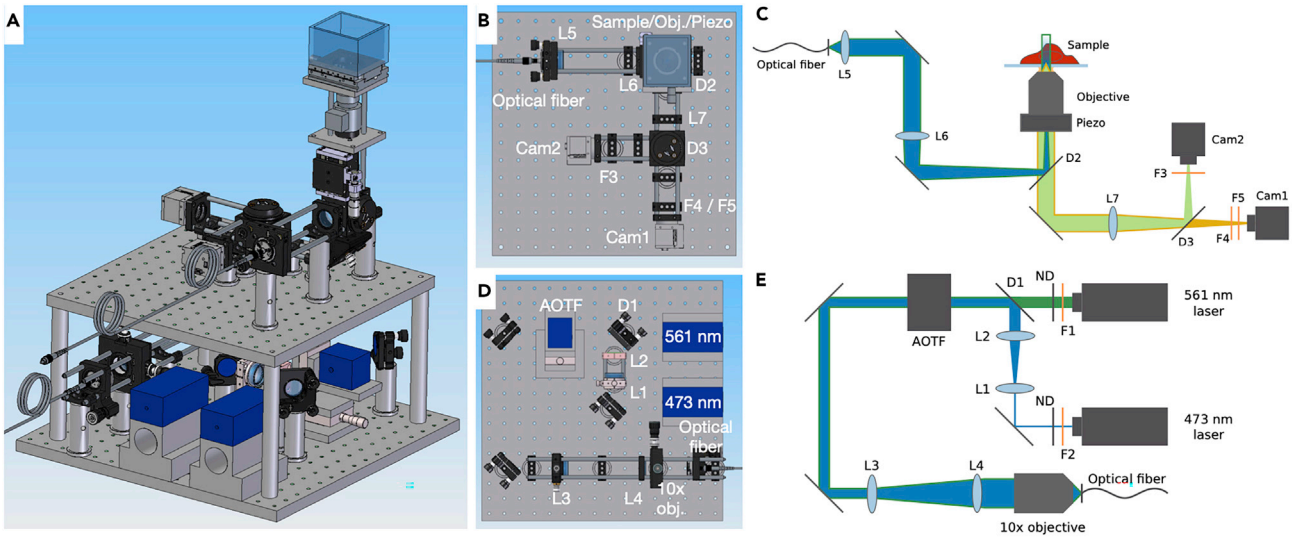

Figure 1. Compact wide-field fluorescence microscope for live-cell imaging of virus-infected cells

(A) 3D computer-aided design (CAD) model of the full microscope system.

(B) Top view of the 3D-CAD model.

(C) Schematics of the fluorescence microscope platform. The laser beams are illuminating the sample in an Epi configuration and the objective lens can be rapidly translated along the optical axis via a piezo stage. The same objective lens is utilized to collect the fluorescence signal, which is separated from the laser light via dichroic mirror D2. A single-tube lens L7 focuses the fluorescence images, which are separated by dichroic mirror D3 onto the cameras Cam1 and Cam2. The inset shows the point spread function (PSF) that can be obtained with this system.

(D) Top view of the 3D-CAD model.

(E) Schematics of the optical layout of the laser combiner. The laser beams are overlaid by dichroic mirror D1 and selectively pass the AOTF. By coupling both beams into a single mode fiber, the transfer of laser light to the microscope platform is simplified and a Gaussian beam profile is obtained.

Figure 1C. This image of a sub-wavelength-sized fluorescent bead serves as the point spread function (PSF) of the microscope system.

A suitable synchronization mechanism between the optics components (AOTF, PiFoc piezo-translation stage for the microscope objective lens, and the cameras) was employed to realize fast 3D dual-color imaging (Figures 2A and 2B). We implemented a customized solution by utilizing the driver box of the piezoelectric translation stage to also provide trigger signals for the other components. To control the image acquisition, the free open-source software μManager[26,27] was used. A synchronization box was built that contains all the required electronics for direct synchronization between the imaging components (cameras, AOTF, piezo driver) by providing trigger signals. For image acquisition, two modes can be used, either a software-synchronized mode (Figure 2A) or a *wavetable* mode (Figure 2B), where synchronization is carried out by the piezo driver. In the software-synchronized mode, all devices are controlled and synchronized by μManager, which makes operating the microscope more flexible and user-friendly. However, latency in the software and signal transfer via the USB bus limits the speed of this mode to 11 fps, which is well below the 100 fps, which could be achieved by the hardware. Thus, direct communication through TTL-style (transistor-transistor logic) trigger pulses, directly sent by the piezo controller to the cameras, are utilized for the wavetable mode, which allows us to reach the full frame rate of 100 fps.

Imaging the transfer of virus particles at the VS between T cells

In order to allow for direct imaging of HIV transfer at the virological synapse (VS) between T cells, a replication-competent clone of HIV-1 was created, containing fusions of viral proteins with fluorescent proteins.[28] The structural protein of HIV-1, Gag, was labeled with mCherry, and the glycoprotein Env was fused to super-folder green fluorescent protein (sfGFP). Jurkat T cells were chosen as the HIV-1 expressing cell line and primary T cells as the target cells (Figure 3, Panel I). Transmitted white-light images (WL) were acquired in order to visualize and identify the cells because both lasers were used to exclusively excite and track the viral proteins.

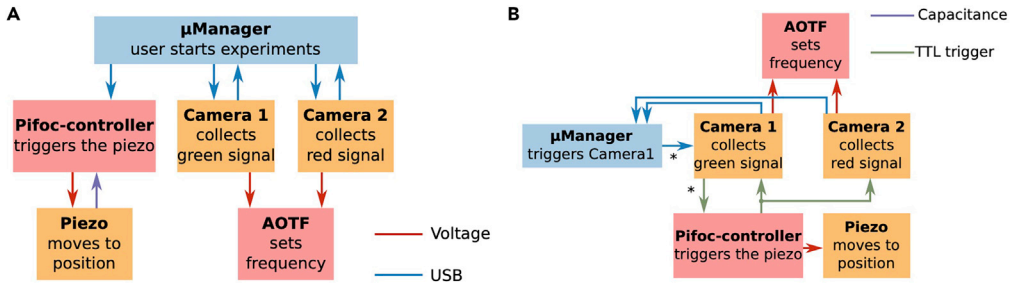

Figure 2. Simplified flowcharts to document the trigger sequence between the electronic devices that control the high-speed imaging process

A Blue box indicates direct access by the user, red boxes indicate hardware control equipment, and yellow boxes illustrate the imaging tools for recording 3D stacks.

(A) In the software-synchronized mode, the user starts the experiment and µManager directly controls the pifoc-controller and the cameras through their USB interface.

(B) In the wavetable mode, µManager initiates Camera1, which sends a trigger signal to the pifoc-controller. This happens only during initiation indicated by *. Afterward, everything is automated by the prestored wavetable on the pifoc-controller.

Contrast enhancement and 3D visualization is achieved during post-processing by applying computational image deconvolution methods to the raw data. This results in a reduced background providing significantly more detail than the unprocessed wide-field images although the spatial resolution is not affected (Figures 3A, 3B, 3D, and 3E). The images collected by the CMOS cameras were processed by the open access Fiji-Plugin[29,30] DeconvolutionLab2.[31] We recorded WL images at the end of each 3D fluorescence image acquisition sequence, which allows us to map host and target cells with respect to each other based on their fluorescence and morphology (Figures 3C and 3F). There is a delay of a few seconds between the acquisition of the last fluorescence image and the acquisition of the WL image. Thus, merging these images does not result in a sufficient overlap because of the high motility of the T cells. Nevertheless, the fluorescent cells can still readily be identified and correlated with the WL images.

The modification of Env and Gag by inserting sfGFP and mCherry, respectively, does not affect the ability of the virus to form VS and engage in cell-to-cell transfer of HIV-1 (see Figure 3).[28,32] In cells expressing viral proteins, Env is mainly localized to intracytoplasmic compartments, whereas Gag attaches to the plasma membrane. Only low intensities of mCherry-Gag are observed in the cytoplasm, which can be clearly seen by the vertical scan through the sample (Figure 3; Videos S1 and S2). Some fluorescent signal from mCherry-Gag can be detected at the top and/or the bottom of the nucleus (Figures 3A and 3B). Nevertheless, the most interesting part is the formation of the VS and the subsequent transfer of virus particles through the VS. The first row of Figure 3 shows the final image of a sequence acquired during a time lapse image acquisition following the transfer of HIV-1 from host cell to target cell (see Figure 4). The images displayed in Figures 3A, 3B, 3D and 3E are maximum intensity projections of full 3D image stacks extending 20 µm along the axial direction that were acquired at a rate of 20 ms per raw image. At a step size of 500 nm, this required 0.8 s to image the entire stack, whereas a step size of 250 nm required 1.6 s for the full stack. In order to best perform the 3D image deconvolution, for all the data displayed in this report, a step size of 250 nm was chosen, resulting in 80 images per 20 µm stack. Maximum intensity projections were chosen in order to best display the data in this manuscript, whereas full 4D animated movies of select HIV-1 transfer processes can be found as Supplementary Video (Figure 4 and Video S3, Figure 5 and Video S4). The second row of Figure 3 displays the final image of the image sequence displayed in Figure 5. We chose to show Figure 3 as the first figure in this manuscript, because it allows us to identify the target cells in Figures 4 and 5.

The transfer of HIV-1 particles at the VS between the host cell and a single target cell can be clearly seen in Figure 4 and Video S3. By comparing Figures 4 with Figure 3, it is obvious that several target cells can simultaneously attach to the infected Jurkat T cell, whereas only a single primary T cell appears to have formed a VS with the host cell. An increased accumulation of sfGFP-Env and mCherry-Gag can be found at the location where the two cells connect, which we identify as the VS (Figure 4D). The subsequent budding and endocytosis of virus particles is visible through the time-lapse recordings (Figures 3E–3G and Video S3).

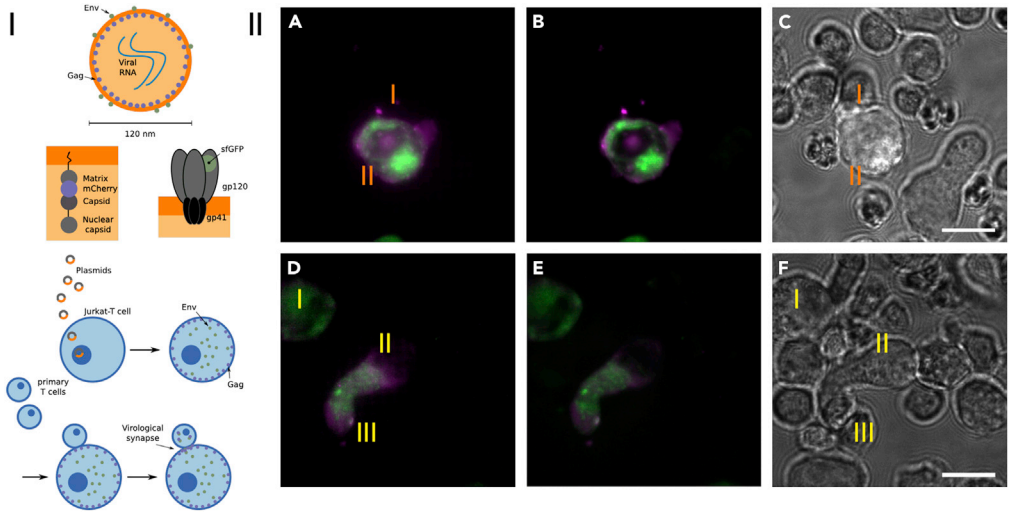

Figure 3. Fluorescent protein labeling strategy and Jurkat-T cells expressing HIV-1 particles

Panel I: scheme of the labeling and experimental strategy for imaging the HIV-1 infection pathway. (Upper row) Single HIV particle. The protein Env is situated at the outer membrane, whereas the structural protein Gag is prominent at the inner membrane and outnumbers Env. (Second row) Structure of Gag with integrated mCherry and structure of Env with integrated sfGFP. (Third row) Experimental outline to investigate the HIV transfer at the VS. First, plasmids encoding HIV with the fusions of mCherry-Gag and sfGFP-Env are introduced in the host Jurkat-T cells by gene transfection. The host cell expresses the HIV proteins, and Gag will attach to the plasma membrane, whereas Env is most prominent in the cytoplasma. (Fourth row) Primary T cells are added, which attach to the Jurkat-T cell. By an interaction of Env with the $CD4^+$ receptors of the target cells, the VS is formed, and the virus assembles at the VS. Subsequent budding leads to a transfer into the target cell. Panel II: fluorescence and wide-field images of the HIV-1 expressing cells: mCherry-Gag (purple) is mostly prominently expressed at the plasma membrane, whereas sfGFP-Env (green) is located in the cytoplasm. The computationally deconvolved images (B and E) exhibit enhanced contrast in comparison to the wide-field images (A and D). Both datasets are maximum intensity z-projections. The corresponding transmitted white-light images (C and F) were recorded several seconds after the acquisition of the fluorescent micrographs. First row: a few target cells appear to have attached to the HIV-1-injected Jurkat T cell (region II), whereas only T cell I appears to have formed a VS with the host cell, which is indicated by the highly concentrated purple signal outside the host cell's cytoplasms, which is likely a vesicle filled with viral protein. The previous initiation of the VS and subsequent budding is shown in the time-lapse image sequence in Figure 3. Second row: high expression of Gag and Env in cell II, whereas cell I indicates almost no Gag. The primary T cell III is attached to cell II via a VS at the uropod. The previous transfer of virus can be seen in the time-lapse image series in Figure 4. Both datasets: 20 ms exposure time per raw frame, 20 μm z stack, Scale bar: 10 μm.

To better visualize this process, we highlighted the budding and transfer by outlining a region of interest (ROI) with a white frame in Figure 4C. This frame is shown as a magnified view in Figure 4D, and the box outlined there is then shown magnified in Figures 4E–4G. Moreover, please note that this is not a singular event and that the transfer of several other sfGFP-Env and mCherry-Gag fusions were also imaged.

T cells can adopt a highly polarized morphology, with a leading edge at the front and swelling at the back end, which is called uropod. Gag can accumulate at the uropod, and thus uninfected T cells preferentially form a VS at the HIV-1 Gag-containing uropod rather than at the leading edge.[33–35] In this context, we also imaged cells, where a high signal of mCherry-Gag was found at the uropod of a Jurkat T cell (Figures 5B and 5D), and by subsequent comparison with the white-light image (Figure 3F), a T cell was confirmed to be present at this location. Hence, we identify this event as the formation of a VS because simultaneously a high signal of sfGFP-Env was also recorded at the same location (Figures 5A, 5C, and Video S4). According to the images acquired at time points 6.48, 14.58, and 21.06 s (see Figure 5), there appear to be two VS present. Due to the lack of a counterstain, it is unclear whether two target T cells are bound to the same Jurkat T cell or not. However, the endocytosis of the virus particles into the target cell appears to transfer different amounts of virus particles, because according to Figure 5D, different signal intensities of the transferred puncta were detected. On the one hand, a strong sfGFP-Env intensity in combination with mCherry-Gag can be found at time point 6.48 s, which is quite prominent over the entire duration of the image sequence. Smaller amounts of both fluorescent protein intensities were also detected, suggesting that only a few virus

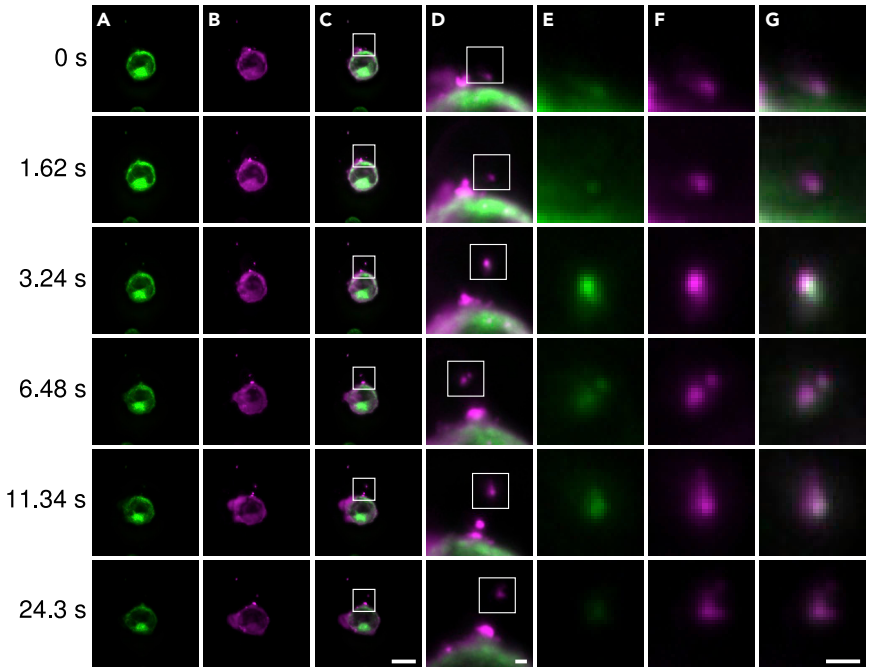

Figure 4. HIV-1 transfer at the VS

The deconvolved widefield fluorescence images are maximum intensity z-projections of a time-lapse movie (20 ms exposure time per raw frame, 20 μm z stack, Video S3). In (A) the sfGFP-Env channel is displayed and in (B) the mCherry-Gag channel can be seen. The enlarged inset (D) of the merged fluorescence images (C) shows the transfer of virus particles through the VS. Other insets (E–G), outlined in (D), show the merged image (G) of the 2 color channels (sfGFP [E] and mCherry [F]) and the correlation of the fluorescent signals is visible. Various transfers of HIV-1 particles can be observed. Scale bars: 10 μm (A–D) and 1 μm (D–G).

particles were transferred. Therefore, to quantify and distinguish between single virus particles, high-speed super-resolution microscopy with the ability to resolve single virus particles in 3D would be best suited to follow this process due to the small size of the virus, which is well below the optical diffraction limit. No currently available super-resolution optical microscopy method does, however, have the ability to resolve and track virus particles in real time in 3D. We are working toward this goal by developing high-speed versions of super-resolution microscopes but have to resolve to showing just images of fixed cells at this time as detailed in the next section below.

Resolving single virus particles by super-resolution structured illumination microscopy

We are currently working toward the development of high-speed super-resolution structured illumination microscopes (SR-SIM), which we view to be one of the few super-resolution optical methods to allow for rapid whole-cell live imaging.[36,37] We have recently made a number of developments toward speeding up the SR-SIM imaging process, while still allowing for instant display of the super-resolved image data, as well as toward the development of more compact and cost effective realizations of SR-SIM.[25,37] In SR-SIM, a low single to double digit number of raw images is acquired, while the sample is illuminated with a diffraction-limited (stripe-like) interference pattern. Computational image reconstruction then results in roughly a doubling of the spatial resolution in x, y, and z.[38,39] For the 3D-SIM measurements shown here, however, different stages of the T cell to T cell HIV-1 transfer process at the VS of *fixed* samples were imaged (Figure 3, Panel I). In contrast to the recordings obtained with the compact, high-speed fluorescence microscope, the plasma membrane and the nucleus were also fluorescently stained to directly identify and image all contributing cells in the super-resolved fluorescence image.

As a first step, the previously obtained results of the live-cell dynamics need to be confirmed in order to guarantee that no deformation is introduced by the chemical fixation process. As already demonstrated in Figure 3, the sfGFP-Env fusion appears mainly in the cytoplasm, whereas the mCherry-Gag complex was predominantly present as an intracellular accumulation at the plasma membrane where the virus

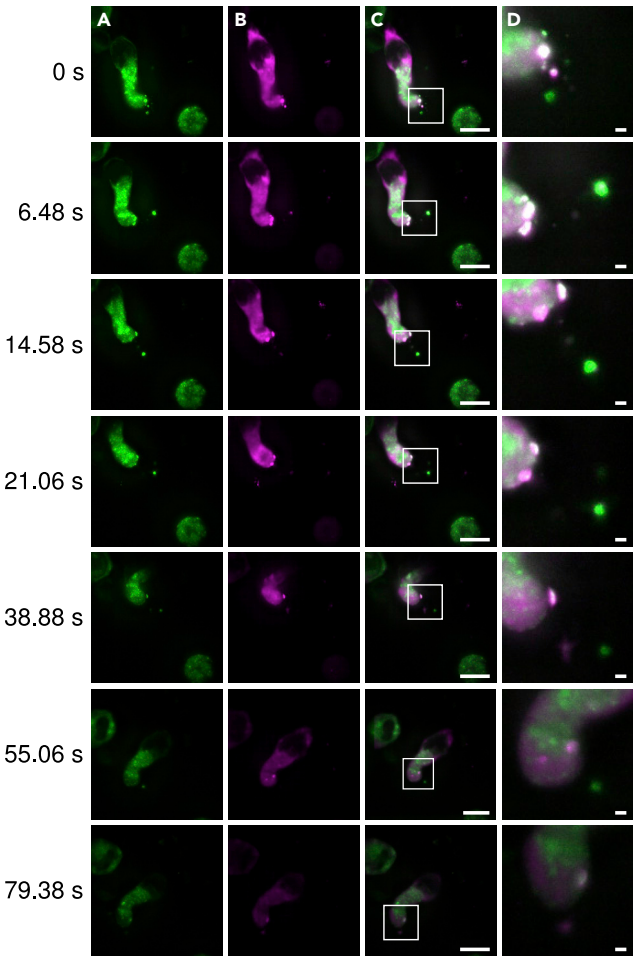

Figure 5. Virus transfer at the VS with clear accumulation of HIV-1 at an uropod

The deconvolved widefield fluorescence images are maximum intensity z-projections of a time-lapse movie (20 ms exposure time per raw frame, 20 μm z stack, Video S4). The merged image (C) of the 2 color channels sfGFP-Env (A) and mCherry-Gag (B) visualizes strong accumulation of the proteins Env and Gag at the VS and the budding of viral material with several endocytosis events by the target cell. Enlarged view of the insets (D) highlighted by white boxes in (C). Scale bars: 10 μm (A–C) and 1 μm (D).

assembles. By additional staining of the plasma membrane, these results can be confirmed by SR-SIM, and the association of mCherry-Gag with the plasma membrane can be even better visualized (Figure 6A). Moreover, as expected, the occurrence of sfGFP-Env at the plasma membrane appears to be very rare, indicating that yet no VS has formed.

After mixing the Jurkat T host cell culture with the target cells, a low fraction of cells (typically approximately 20%) that have formed cell conjugates can be observed.[11,28] The virus-dependent cell-to-cell adhesion increases the localization and assembly of mCherry-Gag at the contact area, where the transfer of the virus can be recorded.[2,7] This attachment, however, is only one step of the successful formation of a VS, and if the sample were to be fixed at that very moment, then no virus particles might have been transferred to the target cells. As seen in Figure 6B, in this example, three primary T cells formed an adhesive structure with a single Jurkat T cell. Gag appears to strongly accumulate at the site of cell-cell adhesion, but no viral fluorescence signal in the target cells can be found. Therefore, we assume that the cell-cell adhesion occurred just prior to fixation or that these adhesion sites are intermittent cell-cell contacts, which do not lead to the formation of a stable VS. The observation of such events required high-throughput and efficient live imaging approaches that are not yet available with current state-of-the-art super-resolution microscopes.[1]

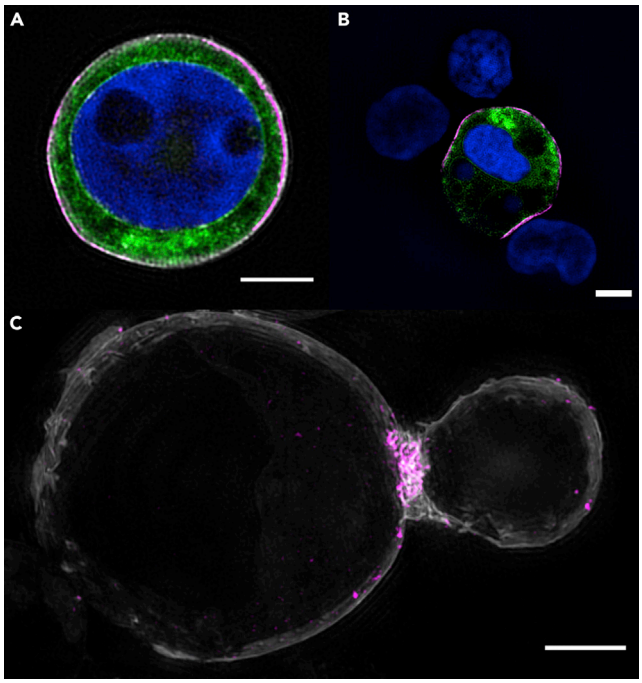

Figure 6. 3D-SIM images of the different stages of the HIV-1 VS transfer process (green, sfGFP-Env; purple, mCherry-Gag; blue, nucleus; white, plasma membrane)

(A) HIV-1 expressing Jurkat-T cell where mCherry-Gag is found to be predominantly localized at the cell's plasma membrane, whereas sfGFP-Env appears to accumulate in the cytoplasm.

(B) Three primary $CD4^+$ T cells (as indicated by the blue nuclei) have attached to the HIV + Jurkat-T cell, but no HIV-1 particles appear to yet sfGFP-Env have been transferred to the target cells. An accumulation of mCherry-Gag at the sites of the T cell nuclei indicates that virological synapses between the infected and uninfected cells have formed.

(C) HIV-1 particles transferred from the donor Jurkat T cell (large cell, to the left) to the previously uninfected primary T cell (small cell, to the right) appear as purple spots in the primary T cell. The accumulation and assembly of virus at the VS adhesive structure between the cells is clearly visible. All images are maximum intensity z-projections of z-stacks with z dimensions of 2.5 μm (a), 2.75 μm (b), and 3.75 μm (c). Scale bar: 3 μm.

Nevertheless, we also successfully imaged transferred HIV-1 particles in target cells (Figure 6C). Here, the VS is clearly defined by the bright fluorescence intensity of mCherry-Gag at the adhesive structure. For this experiment, only a mCherry-Gag construct was utilized, and thus the usage of the membrane stain FastDiO was possible. This dye exhibits improved membrane staining and efficiency in our hands Figure 6C). In addition, according to the images obtained by live imaging (Figures 4 and 5), transfer of mCherry-Gag indicates a high likelihood that sfGFP-Env was also transmitted, as these signals correlate in the early phase of virus transfer. Even single virus particles can be identified at the plasma membrane by SR-SIM, which exemplifies our strong belief that SR-SIM will be the method of choice for live cell imaging at super-resolution in the future.

DISCUSSION

We have demonstrated the feasibility and high sensitivity of a compact wide-field deconvolution fluorescence microscope by live-cell imaging of HIV-1 transfer at the VS between T cells. Just a decade ago, similar experiments required the use of a highly specialized, maintenance intensive and rather expensive optical microscope using a deep-cooled electron-multiplying CCD camera,[2,10] whereas the system described here can image T cells in 2 color channels and at a rate >3x faster at a fraction of the cost (approx. 35 k$ compared with approx. 200 k$). By staining two prominent viral proteins, Env and Gag, the transmission of virus particles at the direct cell-to-cell contact was successfully imaged. In addition, 3D-SIM image stacks of fixed T cell conjugates were recorded for further resolution improvement at the different stages of the infection process and to further identify the spatial correlation of viral proteins with host and target cell

constituents by additional fluorescent dyes, allowing for locating and identifying virus particles in the target cells.

The compact fluorescence microscope was successfully shipped from Germany to New York City, unpacked and installed within just one day to enable the high-speed and high-sensitivity recording of virus transfer between living T cells. Hence, the system proved one of its main purposes, i.e. realizing a compact and cost-effective design along with the robustness and ease of use enabling the shipment and subsequent operation between two continents. The successful installation and operation in an infectious disease research laboratory demonstrated that the system is user friendly and enabled a biology expert postdoctoral researcher at ISMMS to operate the system within a very short period of training (independent operation was possible after 1 day of training; maintenance and minimal adjustments of the system require about 1 week of training for a person with little to no optics background future). Continued operation of the microscope over a period of several months occurred with no need for maintenance of the microscope, which proved the optical system to be stable and reliable. To circumvent the absence of more than 2 color detection channels, a white-light LED source was implemented in the system and was sufficient to identify and map the cells involved in the infection process by white-light transmitted light micrographs. Image processing by DeconvolutionLab2[31] with a pre-determined point spread function (PSF, see the inset in Figure 1C) resulted in the deconvolution of the recorded 3D z-stacks and produced high-quality 3D image reconstructions that were quite sufficient for following and identifying the transmission of HIV-1 between T cells.

Our live cell experiments performed with the compact fluorescence microscope allowed us to follow the transmission of virus particles at the VS in multiple cases. By employing fast 3D image stacks, such events were recorded and after computational image deconvolution the dynamics were visualized with enhanced clarity with comparable spatial resolution and signal-to-noise ratios as previously achieved by spinning disk confocal microscopy.[2] Staining of the viral proteins Env and Gag by fusion with fluorescent proteins was sufficient for their visualization, because it clearly showcased the transmission of virus at the adhesive structure. As expected, Gag appeared to be a beneficial indicator for the formation of the VS, because this protein is most prominent at the cell-to-cell contact. Moreover, the accumulation of Gag at the uropod of a Jurkat T cell was visualized, and the dynamics of virus particles possibly endocytosed by the target cell were detected. Indeed, the live-cell imaging was agreeable but limited in terms of resolution and the number of fluorescent color channels. Although the subsequent acquisition of WL images was helpful in identifying the participating cells, the simultaneous recording of WL data would have been more convenient. This could, however, easily be accomplished by using a color LED or filtering the WL source and adding a third CMOS camera to the microscope in a future redesign.

HIV-1 samples were also imaged by 3D-SIM utilizing four color channels in order to supplement and confirm the experimental findings and deductions made during the live cell imaging experiments. As this is currently limited to imaging fixed samples, the different stages of T cell-to-T cell HIV-1 transfer at the VS could be imaged by 3D-SIM with significant gain in spatial resolution, albeit at time-points predetermined by the time at which the cells were exposed to the fixative. SR-SIM allowed us to resolve single HIV-1 particles with a diameter of about 120 nm. Although some other super-resolution techniques provide even better spatial resolution, these data demonstrate that once a compact, cost-effective, and high-speed SR-SIM will become available that it will be of significant benefit for infectious disease research due to its ability to image conventional fluorescent stains (including fluorescent proteins) at ease, as well as its ability to perform long-term live cell imaging due to the low photon dosage required for the imaging process.[37,40]

The microscope demonstrated here could possibly be improved by further reducing the overall size and costs. Novel concepts such as the use of mobile phones in microscopic imaging[41] and super-resolution microscopy[42] have already been demonstrated and showed that even cellphone cameras can be utilized as sensitive detectors. The cost of laser sources is also ever decreasing. A 50-mW blue laser (488 nm) can now for example be purchased for <1 k$, readily reducing the cost of our instrument by about 6 k$. On the software side, several concepts for real-time deconvolution by parallel computing exist,[43,44] which could be implemented in the compact microscope. This would allow for directly visualizing the images without out-of-focus blur, which would enable an even better control of the experiment already during image acquisition.

The work presented here demonstrates that compact, portable fluorescence microscopy systems can be realized in a rather cost-efficient manner. The system described here has proven its usefulness in demanding infectious disease research. Its continued development and commercialization will provide more researchers in the life sciences to gain access to affordable implementations of advanced fluorescence microscopy. Its portability and ease of use would allow them to operate similar systems in challenging environments (even high-level biosafety laboratories) or remote sites where new viral outbreaks are suspected.

Limitations of the study

- Visualization of the target cell receiving HIV-1 particles during the experiments was limited by the absence of either a third color channel or the simultaneous acquisition of white light images.
- Although raw images can be viewed during the live cell experiments, they are blurred by fluorescence light emitted from regions out of focus, which are excited simultaneously.
- High-quality 3D images are obtained by post-processing image deconvolution, which is time-consuming and prohibits the direct observation of important details of the virus-transfer process already during the experiment.

STAR★METHODS

Detailed methods are provided in the online version of this paper and include the following:

- KEY RESOURCES TABLE
- RESOURCE AVAILABILITY
  - Lead contact
  - Materials availability
  - Data and code availability
- EXPERIMENTAL MODEL AND SUBJECT DETAILS
  - Cell lines
- METHOD DETAILS
  - Live-cell sample preparation
  - Counterstaining of fixed HIV-1 samples
  - Compact wide-field deconvolution microscope
  - Communication scheme between devices
  - Live-cell data acquisition
  - SIM data acquisition
- QUANTIFICATION AND STATISTICAL ANALYSIS
  - Live-cell image processing
  - SIM image processing

SUPPLEMENTAL INFORMATION

Supplemental information can be found online at https://doi.org/10.1016/j.isci.2022.105468.

ACKNOWLEDGMENTS

We thank Andreas Markwirth for help with and discussions about the control electronics of the compact fluorescence microscope. This work was supported by a grant to B.K.C. from the NIH/NIGMS (GM113885) and a subcontract to T.H. The funders had no role in study design, data collection, and interpretation or the decision to submit the work for publication.

AUTHOR CONTRIBUTIONS

A.S. built the compact fluorescence microscope, prepared SIM samples, performed SIM measurements, SIM and deconvolution image processing, and wrote the manuscript. L.W. prepared the live-cell samples and performed live-cell measurements with the compact fluorescence microscope. M.M. set up the electronics and software of the compact fluorescence microscope and helped write the manuscript. W.H. supervised the project and measurements and helped with the analysis and the writing of the manuscript.

B.C. and T.H. conceived of and supervised the project and helped write the manuscript. All authors participated in the reading and editing of the final manuscript.

DECLARATION OF INTERESTS

The authors declare no competing interests.

Received: October 21, 2021
Revised: May 16, 2022
Accepted: October 26, 2022
Published: November 18, 2022

REFERENCES

1. Schermelleh, L., Ferrand, A., Huser, T., Eggeling, C., Sauer, M., Biehlmaier, O., and Drummen, G.P.C. (2019). Super-resolution microscopy demystified. Nat. Cell Biol. *21*, 72–84. https://doi.org/10.1038/s41556-018-0251-8.

2. Hübner, W., McNerney, G.P., Chen, P., Dale, B.M., Gordon, R.E., Chuang, F.Y.S., Li, X.-D., Asmuth, D.M., Huser, T., and Chen, B.K. (2009). Quantitative 3D Video microscopy of HIV transfer across T cell virological synapses. Science *323*, 1743–1747. https://doi.org/10.1126/science.1167525.

3. Power, R.M., and Huisken, J. (2019). Putting advanced microscopy in the hands of biologists. Nat. Methods *16*, 1069–1073. https://doi.org/10.1038/s41592-019-0618-1.

4. Simon, S.I., and Green, C.E. (2005). Molecular mechanics and dynamics of leukocyte recruitment during inflammation. Annu. Rev. Biomed. Eng. *7*, 151–185. https://doi.org/10.1146/annurev.bioeng.7.060804.100423.

5. Batra, H., and Pawar, S. (2019). Current clinical trials update on HIV/AIDS: a systematic review. hivar. *18*, 79–84. https://doi.org/10.5114/hivar.2019.86371.

6. Barouch, D.H. (2008). Challenges in the development of an HIV-1 vaccine. Nature *455*, 613–619. https://doi.org/10.1038/nature07352.

7. Jolly, C., Kashefi, K., Hollinshead, M., and Sattentau, Q.J. (2004). HIV-1 cell to cell transfer across an Env-induced, actin-dependent synapse. J. Exp. Med. *199*, 283–293. https://doi.org/10.1084/jem.20030648.

8. Freed, E.O. (2015). HIV-1 assembly, release and maturation. Nat. Rev. Microbiol. *13*, 484–496. https://doi.org/10.1038/nrmicro3490.

9. Wilen, C.B., Tilton, J.C., and Doms, R.W. (2012). HIV: cell binding and entry. Cold Spring Harb. Perspect. Med. *2*, a006866. https://doi.org/10.1101/cshperspect.a006866.

10. Dale, B.M., McNerney, G.P., Thompson, D.L., Hubner, W., de Los Reyes, K., Chuang, F.Y.S., Huser, T., and Chen, B.K. (2011). Cell-to-cell transfer of HIV-1 via virological synapses leads to endosomal virion maturation that activates viral membrane fusion. Cell Host Microbe *10*, 551–562. https://doi.org/10.1016/j.chom.2011.10.015.

11. Chen, P., Hübner, W., Spinelli, M.A., and Chen, B.K. (2007). Predominant mode of human immunodeficiency virus transfer between T cells is mediated by sustained Env-dependent neutralization-resistant virological synapses. J. Virol. *81*, 12582–12595. https://doi.org/10.1128/JVI.00381-07.

12. Pitrone, P.G., Schindelin, J., Stuyvenberg, L., Preibisch, S., Weber, M., Eliceiri, K.W., Huisken, J., and Tomancak, P. (2013). OpenSPIM: an open-access light-sheet microscopy platform. Nat. Methods *10*, 598–599. https://doi.org/10.1038/nmeth.2507.

13. Holm, T., Klein, T., Löschberger, A., Klamp, T., Wiebusch, G., van de Linde, S., and Sauer, M. (2014). A blueprint for cost-efficient localization microscopy. ChemPhysChem *15*, 651–654. https://doi.org/10.1002/cphc.201300739.

14. Van den Eynde, R., Sandmeyer, A., Vandenberg, W., Duwé, S., Hübner, W., Huser, T., Dedecker, P., and Müller, M. (2019). Quantitative comparison of camera technologies for cost-effective super-resolution optical fluctuation imaging (SOFI). J. Phys. Photonics *1*, 044001. https://doi.org/10.1088/2515-7647/ab36ae.

15. Diekmann, R., Till, K., Müller, M., Simonis, M., Schüttpelz, M., and Huser, T. (2017). Characterization of an industry-grade CMOS camera well suited for single molecule localization microscopy – high performance super-resolution at low cost. Sci. Rep. *7*, 14425. https://doi.org/10.1038/s41598-017-14762-6.

16. Zhang, Y.S., Ribas, J., Nadhman, A., Aleman, J., Selimović, Š., Lesher-Perez, S.C., Wang, T., Manoharan, V., Shin, S.-R., Damilano, A., et al. (2015). A cost-effective fluorescence mini-microscope for biomedical applications. Lab Chip *15*, 3661–3669. https://doi.org/10.1039/c5lc00666j.

17. Yamagata, K., Iwamoto, D., Terashita, Y., Li, C., Wakayama, S., Hayashi-Takanaka, Y., Kimura, H., Saeki, K., and Wakayama, T. (2012). Fluorescence cell imaging and manipulation using conventional halogen lamp microscopy. PLoS One *7*, e31638. https://doi.org/10.1371/journal.pone.0031638.

18. Schaefer, S., Boehm, S.A., and Chau, K.J. (2012). Automated, portable, low-cost bright-field and fluorescence microscope with autofocus and autoscanning capabilities. Appl. Opt. *51*, 2581–2588. https://doi.org/10.1364/AO.51.002581.

19. Stewart, C., and Giannini, J. (2016). Inexpensive, open source epifluorescence microscopes. J. Chem. Educ. *93*, 1310–1315. https://doi.org/10.1021/acs.jchemed.5b00984.

20. Hasan, M.M., Alam, M.W., Wahid, K.A., Miah, S., and Lukong, K.E. (2016). A low-cost digital microscope with real-time fluorescent imaging capability. PLoS One *11*, e0167863. https://doi.org/10.1371/journal.pone.0167863.

21. Liu, Y., Rollins, A.M., Levenson, R.M., Fereidouni, F., and Jenkins, M.W. (2021). Pocket MUSE: an affordable, versatile and high-performance fluorescence microscope using a smartphone. Commun. Biol. *4*, 334–414. https://doi.org/10.1038/s42003-021-01860-5.

22. Diederich, B., Lachmann, R., Carlstedt, S., Marsikova, B., Wang, H., Uwurukundo, X., Mosig, A.S., and Heintzmann, R. (2020). A versatile and customizable low-cost 3D-printed open standard for microscopic imaging. Nat. Commun. *11*, 5979. https://doi.org/10.1038/s41467-020-19447-9.

23. Mao, H., Diekmann, R., Liang, H.P.H., Cogger, V.C., Le Couteur, D.G., Lockwood, G.P., Hunt, N.J., Schüttpelz, M., Huser, T.R., Chen, V.M., and McCourt, P.A. (2019). Cost-efficient nanoscopy reveals nanoscale architecture of liver cells and platelets. Nanophotonics *8*, 1299–1313. https://doi.org/10.1515/nanoph-2019-0066.

24. Babcock, H.P. (2018). Multiplane and spectrally-resolved single molecule localization microscopy with industrial grade CMOS cameras. Sci. Rep. *8*, 1726. https://doi.org/10.1038/s41598-018-19981-z.

25. Sandmeyer, A., Lachetta, M., Sandmeyer, H., Hübner, W., Huser, T., and Müller, M. (2021). Cost-effective live cell structured illumination microscopy with video-rate imaging. ACS Photonics *8*, 1639–1648. https://doi.org/10.1021/acsphotonics.0c01937.

26. Edelstein, A., Amodaj, N., Hoover, K., Vale, R., and Stuurman, N. (2010). Computer

control of microscopes using μManager. Curr. Protoc. Mol. Biol. *92*, 14–20. https://doi.org/10.1002/0471142727.mb1420s92.

27. Edelstein, A.D., Tsuchida, M.A., Amodaj, N., Pinkard, H., Vale, R.D., and Stuurman, N. (2014). Advanced methods of microscope control using μManager software. J. Biol. Methods *1*, e10. https://doi.org/10.14440/jbm.2014.36.

28. Hübner, W., Chen, P., Del Portillo, A., Liu, Y., Gordon, R.E., and Chen, B.K. (2007). Sequence of human immunodeficiency virus type 1 (HIV-1) Gag localization and oligomerization monitored with live confocal imaging of a replication-competent, fluorescently tagged HIV-1. J. Virol. *81*, 12596–12607. https://doi.org/10.1128/JVI.01088-07.

29. Schneider, C.A., Rasband, W.S., and Eliceiri, K.W. (2012). NIH Image to ImageJ: 25 years of image analysis. Nat. Methods *9*, 671–675. https://doi.org/10.1038/nmeth.2089.

30. Schindelin, J., Arganda-Carreras, I., Frise, E., Kaynig, V., Longair, M., Pietzsch, T., Preibisch, S., Rueden, C., Saalfeld, S., Schmid, B., et al. (2012). Fiji: an open-source platform for biological-image analysis. Nat. Methods *9*, 676–682. https://doi.org/10.1038/nmeth.2019.

31. Sage, D., Donati, L., Soulez, F., Fortun, D., Schmit, G., Seitz, A., Guiet, R., Vonesch, C., and Unser, M. (2017). DeconvolutionLab2: an open-source software for deconvolution microscopy. Methods *115*, 28–41. https://doi.org/10.1016/j.ymeth.2016.12.015.

32. Nakane, S., Iwamoto, A., and Matsuda, Z. (2015). The V4 and V5 variable loops of HIV-1 envelope glycoprotein are tolerant to insertion of green fluorescent protein and are useful targets for labeling. J. Biol. Chem. *290*, 15279–15291. https://doi.org/10.1074/jbc.M114.628610.

33. Jolly, C. (2010). T cell polarization at the virological synapse. Viruses *2*, 1261–1278. https://doi.org/10.3390/v2061261.

34. Llewellyn, G.N., Grover, J.R., Olety, B., and Ono, A. (2013). HIV-1 Gag associates with specific uropod-directed microdomains in a manner dependent on its MA highly basic region. J. Virol. *87*, 6441–6454. https://doi.org/10.1128/JVI.00040-13.

35. Llewellyn, G.N., Hogue, I.B., Grover, J.R., and Ono, A. (2010). Nucleocapsid promotes localization of HIV-1 Gag to uropods that participate in virological synapses between T cells. PLoS Pathog. *6*, e1001167. https://doi.org/10.1371/journal.ppat.1001167.

36. Heintzmann, R., and Huser, T. (2017). Super-resolution structured illumination microscopy. Chem. Rev. *117*, 13890–13908. https://doi.org/10.1021/acs.chemrev.7b00218.

37. Markwirth, A., Lachetta, M., Mönkemöller, V., Heintzmann, R., Hübner, W., Huser, T., and Müller, M. (2019). Video-rate multi-color structured illumination microscopy with simultaneous real-time reconstruction. Nat. Commun. *10*, 4315. https://doi.org/10.1038/s41467-019-12165-x.

38. Gustafsson, M.G.L., Shao, L., Carlton, P.M., Wang, C.J.R., Golubovskaya, I.N., Cande, W.Z., Agard, D.A., and Sedat, J.W. (2008). Three-dimensional resolution doubling in wide-field fluorescence microscopy by structured illumination. Biophys. J. *94*, 4957–4970. https://doi.org/10.1529/biophysj.107.120345.

39. Müller, M., Mönkemöller, V., Hennig, S., Hübner, W., and Huser, T. (2016). Open-source image reconstruction of super-resolution structured illumination microscopy data in ImageJ. Nat. Commun. *7*, 10980. https://doi.org/10.1038/ncomms10980.

40. Huang, X., Fan, J., Li, L., Liu, H., Wu, R., Wu, Y., Wei, L., Mao, H., Lal, A., Xi, P., et al. (2018). Fast, long-term, super-resolution imaging with Hessian structured illumination microscopy. Nat. Biotechnol. *36*, 451–459. https://doi.org/10.1038/nbt.4115.

41. Orth, A., Wilson, E.R., Thompson, J.G., and Gibson, B.C. (2018). A dual-mode mobile phone microscope using the onboard camera flash and ambient light. Sci. Rep. *8*, 3298. https://doi.org/10.1038/s41598-018-21543-2.

42. Diederich, B., Then, P., Jügler, A., Förster, R., and Heintzmann, R. (2019). cellSTORM—cost-effective super-resolution on a cellphone using dSTORM. PLoS One *14*, e0209827. https://doi.org/10.1371/journal.pone.0209827.

43. Bruce, M.A., and Butte, M.J. (2013). Real-time GPU-based 3D deconvolution. Opt Express *21*, 4766–4773. https://doi.org/10.1364/OE.21.004766.

44. Schmid, B., and Huisken, J. (2015). Real-time multi-view deconvolution. Bioinformatics *31*, 3398–3400. https://doi.org/10.1093/bioinformatics/btv387.

45. Kirshner, H., Aguet, F., Sage, D., and Unser, M. (2013). 3-D PSF fitting for fluorescence microscopy: implementation and localization application. J. Microsc. *249*, 13–25. https://doi.org/10.1111/j.1365-2818.2012.03675.x.

STAR★METHODS

KEY RESOURCES TABLE

REAGENT or RESOURCE	SOURCE	IDENTIFIER
Biological samples		
Primary CD4$^+$ T cells	human peripheral blood from deidentified HIV-negative blood donors, through the New York Blood Center	
Deposited data		
Raw and analyzed image data	This paper	https://doi.org/10.5281/zenodo.7215750
Experimental models: Cell lines		
Human: Jurkat Clone E6.1	ATTC	TIB-152
Recombinant DNA		
pNL4-3 Gag-iCherry	Benjamin K. Chen	
pNL4-3 Env-V4.1-sfGFP	Benjamin K. Chen	
Software and algorithms		
Micro-Manager v1.4	http://micro-manager.org	https://doi.org/10.14440/jbm.2014.36
Fiji	http://fiji.sc	https://doi.org/10.1038/nmeth.2019
SoftWorX v7.0	GE Healthcare	
DeconvolutionLab2	http://bigwww.epfl.ch/deconvolution/deconvolutionlab2/	https://doi.org/10.1016/j.ymeth.2016.12.015

RESOURCE AVAILABILITY

Lead contact

Further information and requests for resources should be directed to the lead contact, Thomas Huser (thomas.huser@physik.uni-bielefeld.de).

Materials availability

This study did not generate new unique wet-lab reagents.

Data and code availability

- The image datasets supporting the current study have been deposited at Zenodo and are publicly available as of the date of publication. The DOI is listed in the key resources table.
- This paper does not report original code.
- Any additional information required to reanalyze the data reported in this paper is available from the lead contact upon request.

EXPERIMENTAL MODEL AND SUBJECT DETAILS

Cell lines

Jurkat T cells (host cells) were transfected with the plasmids encoding mCherry-Gag and sfGFP-Env and incubated overnight at 37°C. The structural protein of HIV-1, Gag, can be labeled through internal insertion of a sequence coding for the fluorescent protein mCherry between the section corresponding to the Matrix and Capsid domain (Figure 3, Panel I).[28] This results in an efficient way of fluorescent labeling assembly sites and immature as well as mature viral particles without impairing much of the infectivity rates of such constructs. Double labeling is possible with the use of other fluorescent proteins fused to other viral components. An insertion of sequences coding for super-folding GFP (sfGFP) in the gp120 subdomain of Env at variable loop four was used as the second fluorescent protein (Figure 3, Panel I).[32] After the transfection of the different full replication competent viral genomes containing the fusion of sfGFP-Env and

mCherry-Gag, Jurkat T cells were mixed with a double amount of primary $CD4^+$ T cells (Figure 3, Panel I). These cells were isolated from HIV-1 negative donors previously. While a majority has dismissed in forming a VS, 10%–20% will show a strong adhesion between HIV + Jurkat-T cells and one or more primary $CD4^+$ T cells.[2]

METHOD DETAILS

Live-cell sample preparation

Primary $CD4^+$ T cells were obtained from human peripheral blood from deidentified HIV-negative blood donors, through the New York Blood Center and $CD4^+$ cells isolated by negative selection with a Miltenyi CD4 T cell isolation kit II (Miltenyi Biotec). Next, primary T cells (target cell) and Jurkat T cells were mixed at a ratio of approximately 2:1 and cocultured at 37°C. After 3 h, the mixture was fixed with 4% PFA (paraformaldehyde) in PBS (PBS).

Counterstaining of fixed HIV-1 samples

The fixed sample mixture of HIV + Jurkat T cells and primary T cells was suspended and stored in an Eppendorf 1mL tube. The tube had to be flipped carefully in order to dilute the suspended cells. Next, the tip of a pipette was cut off and used to remove 20 µL of the sample solution. The droplet was placed on a ø12mm coverslip and incubated at room temperature in the dark for 20 min. For the membrane stain, WGA647 (0.1 µL, 1:2000 solution) was used if sfGFP was present, otherwise FastDiO (1 µL, stock solution) was used. In both cases, the membrane dyes were incubated for 10 min within the sample mixture at room temperature in the dark. Next, the solution was completely removed, so that the coverslip was nearly dry. At the location of the cells, 4 µL Vectashield including DAPI (Vector Laboratories, #H1200) was added and a cover glass was placed on top without inducing bubbles in the mounting medium. Lastly, the sample was sealed with nail polish.

Compact wide-field deconvolution microscope

The compact wide-field microscope was equipped with a 473 nm, 50 mW diode laser (Spectra Physics Excelsior, USA) and a 561nm, 20 mW diode laser (Coherent Compass, Germany) for excitation. An acousto-optic tunable filter ('AOTF', AA OptoElectronic AOTF, France) was used to enable fast switching of the laser, to restrict illuminating the sample just during data acquisition, and to reduce photobleaching effects to a minimum. After passing through the AOTF, the excitation beam is coupled into a single mode fiber and then focused to the back focal plane of the objective lens (UPLSAPO60XO 60×, 1.35 NA oil objective, Olympus), which is held on a piezo-electric stage (PiFoc, Physik Instrumente, Germany) for fast displacement along the optical axis. The fluorescence signal was collected with the same objective lens and the emission was separated from the excitation source by a dichroic mirror (HC Dual Line—BSR488/561, Semrock, USA). The fluorescence signals were further separated by an additional dichroic mirror (HC BS 560i, Semrock, USA). The fluorescence images are focused on two industry-grade CMOS cameras (IDSμEye UI-3060CP-*M*-GL Rev.2) using a 180 mm tube lens and after passing additional emission filters (BP 520/77 (#87-749), BP 620/60 (#33-910), BP 591.5/49 (#67-034), all Edmund Optics), resulting in an overall projected pixel size of 97 nm.

Communication scheme between devices

In the software-synchronized mode, the user starts the experiment by setting parameters for the data acquisition with µManager (Figure 2A). The program sends a USB signal to the connected pifoc-controller which is the amplifier and control loop for the z-piezo. This z-piezo thus moves the objective to the required location along the optical axis and an image can be recorded. A capacitance distance measurement controls a feedback loop in the pifoc-controller, which thus can check if a position has been reached and actively maintain it. The controller also sends a confirmation of the completed movement to MicroManager, which in turn acquired images on the cameras. The cameras automatically generate a hardware trigger signal for the AOTF controller, which generates the required frequencies, so that the lasers can illuminate the sample and the cameras can collect the fluorescent signal. Since each z-step and image acquisition requires multiple passes through USB bus communication, latencies inherent to this communication accumulate and limit the maximum frame rate to about 11 fps.

In the wavetable mode, the achieved frame can be increased to the hardware limit of 100 fps by a direct communication between the pifoc-controller and the cameras (Figure 2B). Here, the z-piezo is controlled

directly by firmware running on its controller, and a so-called wavetable, which holds all the position and trigger signals, is stored on and run by the pifoc-controller. Therefore, no high latency synchronization through the USB bus is required (image data of course is still send via USB, but this does not impact latency). In detail, when the user initiates a loop, μManager only generates a single trigger signal, which is send by Camera1 to the pifoc-controller. This starts the prestored wavetable, which in turn generates hardware trigger signals for each camera at each z step. Although high frame rates are achieved, the usage of this mode currently requires an experienced user, as the wavetables require a somewhat involved setup, which as of yet it not directly accessible through Micro-Manager. Additionally, some frames might be lost during the acquisition. Thus, experiments that are not time-critical are done by only using μManager to control all devices.

For the direct communication between the pifoc-controller, cameras and AOTF a synchronization box was designed, mainly containing voltage shifters so that all trigger signals are send to their corresponding targets at the correct level (TTL, LVTTL, 5V/10V AOTF). The signal of the pifoc-controller has to be level-shifted by an additional power supply and level shifter in order to reliably trigger the optocouplers of the cameras that start the exposure. On exposure, signal is sent from the cameras to the AOTF to let the lasers pass and illuminate the sample. A stabilized 5 V or 10V voltage is passed to the output optocouplers provided by the cameras. Two switches allow to toggle between the voltages for both cameras, so when set to 10 V, the full voltage reaches the AOTF and the whole laser power passes. Otherwise, if 5V is applied, only half of the laser power reaches the sample. This provides an easy mean to attenuate the laser.

Live-cell data acquisition

The data acquisition of 3D fluorescence image stacks with subsequent image deconvolution starts by turning on the heating stage if live-cell experiments are carried out. After approximately 10 min, the desired temperature of 37°C is reached, and immersion oil (Zeiss, n = 1.518) and the sample are placed on the objective lens and heating stage. The heating stage itself is mounted on a xy-stage with manual micrometer-screws, so that the user can maneuver the sample in the lateral direction. Another micrometer-screw is mounted at the PiFoc piezo stage to initially focus the sample. Imaging parameters for the cameras (exposure time and frame rate) and the z-piezo (z-stepsize and total scan volume) can be set from within the μManager software package.[26,27] Furthermore, the z-piezo can be used to find the perfect focus since smaller steps in axial direction are available. To adjust the laser power, 10% ND-filters can be placed in front of the lasers. Additionally, the power can be reduced by 50% by an attenuation switch on the synchronization box, switching between two voltage levels send to the AOTF. A combination of the ND-filters and the electric attenuation is also possible.

SIM data acquisition

The fixed samples were imaged with a commercial SR-SIM microscope (DeltaVision|OMX v4, GE Healthcare, USA). 3D-SIM stacks were recorded with the z-range indicated in Figure 6.

QUANTIFICATION AND STATISTICAL ANALYSIS

Live-cell image processing

For post-processing image deconvolution, ImageJ/Fiji[29,30] and additional plugins were used. First, an ideal PSF according to the Born-Wolf model was generated by using the plugin PSF Generator.[45] The recorded image stack needs to be split in the individual color channels for the deconvolution step, which was accomplished by utilizing the plugin DeconvolutionLab2.[31] The Richardson-Lucy algorithm was chosen as the image reconstruction method and 20 iterations were chosen as sufficient. In order to register the color channels, a TetraSpeck (TS) 200nm bead slide was recorded as calibration sample.

SIM image processing

3D-SIM stacks were reconstructed with the manufacturer supplied software (SoftWorX, GE Healthcare, USA) to obtain super-resolved fluorescence images. Further image processing, such as maximum intensity z-projection were also carried out with the manufacturer supplied software.